The Astrophysical Journal Letters, 730:L29 (6pp), 2011 April 1 doi:10.1088/0004-637X/730/2/L29

COMMON WARM DUST TEMPERATURES AROUND MAIN-SEQUENCE STARS

Farisa Y. Morales[1,2], G. H. Rieke[3], M. W. Werner[1], G. Bryden[1,4], K. R. Stapelfeldt[1], and K. Y. L. Su[3]
[1] Jet Propulsion Laboratory, California Institute of Technology, 4800 Oak Grove Drive, Pasadena, CA 91109, USA; Farisa@jpl.nasa.gov
[2] Department of Physics and Astronomy, University of Southern California, Los Angeles, CA 90089-0484, USA
[3] Steward Observatory, University of Arizona, 933 North Cherry Avenue, Tucson, AZ 85721, USA
[4] NExScI, NASA Exoplanet Science Institute, California Institute of Technology, 770 South Wilson Avenue, Pasadena, CA 91125, USA
Received 2010 December 15; accepted 2011 February 21; published 2011 March 9

ABSTRACT

We compare the properties of warm dust emission from a sample of main-sequence A-type stars (B8–A7) to those of dust around solar-type stars (F5–K0) with similar *Spitzer Space Telescope* Infrared Spectrograph/MIPS data and similar ages. Both samples include stars with sources with infrared spectral energy distributions that show evidence of multiple components. Over the range of stellar types considered, we obtain nearly the same characteristic dust temperatures (∼190 K and ∼60 K for the inner and outer dust components, respectively)—slightly above the ice evaporation temperature for the inner belts. The warm inner dust temperature is readily explained if populations of small grains are being released by sublimation of ice from icy planetesimals. Evaporation of low-eccentricity icy bodies at ∼150 K can deposit particles into an inner/warm belt, where the small grains are heated to $T_{\rm dust} \sim 190$ K. Alternatively, enhanced collisional processing of an asteroid belt-like system of parent planetesimals just interior to the snow line may account for the observed uniformity in dust temperature. The similarity in temperature of the warmer dust across our B8-K0 stellar sample strongly suggests that dust-producing planetesimals are not found at similar radial locations around all stars, but that dust production is favored at a characteristic temperature horizon.

Key words: circumstellar matter – infrared: stars – interplanetary medium

1. INTRODUCTION

Since their discovery by the *Infrared Astronomical Satellite* (*IRAS*) in the 1980s (Aumann et al. 1984), we have identified hundreds of circumstellar debris disks around mature stars; the present challenge is to relate their properties to specific phases in the evolution of planetary systems. In a few well-studied examples, the rings are shepherded by planets that maintain sharp inner edges to their structures (e.g., Fomalhaut and HR 8799; Kalas et al. 2008; Marois et al. 2008). Systems with warm dust have been considered rare (Smith et al. 2008; Rhee et al. 2008). However, *Spitzer Space Telescope* (Werner et al. 2004) observations using the Infrared Spectrograph (IRS; Houck et al. 2004) and Multiband Imaging Photometer (MIPS; Rieke et al. 2004) have often revealed warm dust (∼200 K; Morales et al. 2009) and evidence of multiple radial components (e.g., Hillenbrand et al. 2008; Chen et al. 2009; Su et al. 2009). Here, we discuss a sample of ∼70 debris systems where *Spitzer* reveals regions similar in temperature to our asteroid belt and the interior zodiacal cloud (150–250 K; Low et al. 1984; Kelsall et al. 1998).

In this Letter, we address the nature of the warm emission by comparing the characteristic temperatures of warm dust around A- and solar-type stars (the A-type sample covers a stellar spectral range from B8 to A7, and the solar-type between F5 and K0). We describe our sample selection in Section 2 and the *Spitzer* IRS and MIPS data in Section 3. Section 4 describes our fitting procedure and principal result—that there is a remarkable similarity in the warm dust temperature for the great majority of systems. In Section 5, we explore possible mechanisms for dust production at a characteristic inner belt temperature. Section 6 summarizes our findings.

2. SAMPLE SELECTION

Our goal is to compare the results of Morales et al. (2009, hereafter M09), who studied mid-IR excess characteristics in a sample of 50 A-type stars, with a similar sample but around solar-type stars. Because of this direct comparison, we restrict the solar-type sample to stars with ages less than 1 Gyr (roughly the main-sequence lifetime of an A star). Both samples are selected on the basis of MIPS 24 μm excess emission $\geqslant$10% above that expected from the stellar photosphere.

The solar-type stars were observed with MIPS under *Spitzer* GTO programs (PIDs) 148 and 41 (Carpenter et al. 2009; Trilling et al. 2008). The final solar-type sample consists of 19 debris disks around stars of masses within 20% of $M_{\odot}$, distances of 14–54 pc, and ranging in age from 40 to 900 Myr.[5]

Tables 1 and 2 list the observed solar- and A-type samples, the measured MIPS fluxes, and properties derived for the circumstellar dust based on the fitting procedure described below and following the steps outlined in M09. Note that with median values $\sim 10^{-5}$ to 10^{-4} for $L_{\rm dust}/L_{\star}$, these dust clouds are more substantial than the $\sim 10^{-7}$ to 10^{-6} inferred for the circumsolar zodiacal cloud today (Backman et al. 1995; Stern 1996; Fixsen & Dwek 2002).

3. OBSERVATIONS AND DATA REDUCTION

3.1. IRS Spectra

All stars were observed with the low spectral resolution modules of the IRS spectrograph ($\lambda/\Delta\lambda \sim 100$). The solar-type sample has spectroscopy from 7.5 to 35.0 μm (compared with 5.2–35.0 μm for the A stars). Each spectrum contains several components: short–low module (SL1; 7.5–14.5 μm) and two orders from long–low (LL1 and LL2; 14.0–35.0 μm).

Most of the IRS data for the solar-type sources were obtained under *Spitzer* PID 148 and are published in Carpenter et al. (2009). The A-type star-disk IRS spectroscopy (mostly obtained under PID 20132) is described in M09, and the data reduction for the solar-type stars was similar. We use post-basic calibrated data (post-BCDs) from the Spitzer Science Center (SSC) IRS

[5] Age estimates are from cluster and moving group membership, or estimated from chromospheric emission using the calibration of Mamajek & Hillenbrand (2008).

Table 1
Solar-type Sample: Stellar Properties and Fitting Results

Name	Spectral Type	Age[a] (Myr)	Dist. (pc)	$F_{\nu,24}$[b] (mJy)	$F_{\nu,70}$[b] (mJy)	$F_{24}/F_\star$	$F_{70}/F_\star$	$L_{d,\mathrm{warm}}/L_\star$	$L_{d,\mathrm{cold}}/L_\star$	T_{warm} (K)	T_{cold} (K)	t_{coll} (10^3 yr)	$M_{\mathrm{min,in}}$ (10^{-8} $M_\oplus$)	M_{pl} (10^{-3} $M_\oplus$)
HD 000166	K0Ve	456	13.7	157.4 ± 0.8	106.0 ± 3.5	1.26	8.1	6.7×10^{-5}	6.9×10^{-5}	216	63	0.1	0.2	14
HD 000377	G2V	270	39.8	36.3 ± 0.2	170.1 ± 6.3	1.55	70.1	7.0×10^{-5}	4.5×10^{-4}	183	52	0.2	2	32
HD 012039	G4V	40	42.4	25.3 ± 0.1	0.2 ± 4.9[c]	1.48	...	1.2×10^{-4}	...	138	...	0.2	9	15
HD 013246	F8V C	260	45	45.9 ± 0.2	0.2 ± 4.2[c]	2.07	...	2.3×10^{-4}	...	191	...	0.1	22	728
HD 019668	G0V	200	40.2	18.5 ± 0.1	0.2 ± 5.5[c]	1.43	...	1.2×10^{-4}	...	220	...	0.1	4	88
HD 043989	G0	120	49.8	20.7 ± 0.1	10.3 ± 5.2[c]	1.28	...	6.2×10^{-5}	...	199	...	0.2	3	17
HD 060737	G0	430	38.3	23.7 ± 0.1	14.7 ± 5.5[c]	1.17	...	4.2×10^{-5}	...	172	...	0.5	4	32
HD 061005	G8Vk+	220	34.5	45.2 ± 0.2	637.5 ± 6.2	2.48	348.2	1.5×10^{-4}	2.8×10^{-3}	152	54	0.1	4	68
HD 072687	G5V	280	45.7	18.7 ± 0.1	0.3 ± 4.7[c]	1.41	...	1.2×10^{-4}	...	183	...	0.1	2	68
HD 085301	G5	630	32.2	36.4 ± 0.2	32.6 ± 4.0	1.54	12.9	1.1×10^{-4}	7.9×10^{-5}	177	61	0.1	3	146
HD 090905	F5	440	31.6	49.2 ± 0.3	0.3 ± 6.2[c]	1.24	...	4.4×10^{-5}	...	196	...	0.5	9	76
HD 104860	F8	200	47.9	19.6 ± 0.1	188.3 ± 3.9	1.18	110.6	2.8×10^{-5}	6.1×10^{-4}	212	47	0.5	2	7
HD 107146	G2V	350	28.5	61.4 ± 0.3	705.7 ± 16.4	1.52	165.5	1.3×10^{-4}	1.1×10^{-3}	117	48	0.4	29	236
HD 118972	K0Vk:	399	15.6	86.2 ± 0.5	35.4 ± 3.5	1.21	4.5	4.4×10^{-5}	...	99[d]	...	1.2	4	13
HD 145229	G0	900	33	31.2 ± 0.2	66.4 ± 4.4	1.17	23.9	4.4×10^{-5}	1.3×10^{-4}	162	51	0.6	5	75
HD 183216	F8.5VFe+04	840	34.7	39.1 ± 0.2	24.5 ± 5.7	1.22	7.3	2.7×10^{-5}	4.9×10^{-5}	184	68	0.7	3	32
HE 000848	F9V	90	36.5	4.6 ± 0.0	0.3 ± 5.9[c]	1.74	...	1.5×10^{-4}	...	156	...	0.2	25	108
HII 001101	G0V	115	54.1	3.7 ± 0.0	6.1 ± 6.6[c]	1.81	...	2.4×10^{-4}	...	155	...	0.1	31	306
HIP 06276	G9Vk:	90	35.1	19.3 ± 0.1	3.2 ± 5.3[c]	1.31	...	6.3×10^{-5}	...	175	...	0.2	1	4

Notes.
[a] Age estimates as in Rieke et al. (2005).
[b] Measured MIPS photometry, not color corrected.
[c] Upper limit.
[d] IRS+MIPS 70 μm excess well fit by a single component.

data reduction pipeline version S18.0.0, in which the spectra are extracted using a variable aperture width that scales with the width of the instrumental point-spread function. The co-added spectra are calibrated assuming a point source, and background subtracted by differencing the two nodding positions (see the IRS manual for further details). Beyond the post-BCD spectra, we have performed several additional data reduction and analysis steps, such as stitching and trimming of the spectra, using IDL as described in M09.

3.2. MIPS Photometry

Our debris disk samples have been observed by MIPS at both 24 and 70 μm. While the results of these photometric measurements have already been published, they do not come from a single program. Therefore, we re-reduced all MIPS data for uniformity as in M09. All MIPS detections (signal-to-noise ratio >3), 24 μm and 70 μm, are in excess of the stellar photosphere (the predicted level of photospheric emission is based on the NextGen models used in the fitting procedure described in Section 4.1) at excess levels of 1.1–4.1 times the photopsheric value at 24 μm, and from 1.6 to 350 times above at 70 μm (Table 1). 28 of the 50 A-type disks and 9 of the 19 solar-type are detected by MIPS at 70 μm; the rest have upper limits. All 24 μm measurements of excesses are confirmed by the *Spitzer*/IRS spectra. Even in cases where the photometric excess is only ∼10%, the shape of the spectrum as measured by IRS clearly shows dust emission above the photospheric contribution.

4. ANALYSIS AND RESULTS

4.1. SED Fitting Procedure

Motivated by the shape of the excess spectra, and the presence of multiple separate components in a number of well-studied systems (e.g., Fomalhaut (Stapelfeldt et al. 2004), HR 8799 (Su et al. 2009), and our solar system), we fit the mid-IR data out to 70 μm by combining a NextGen model for the stellar photosphere fixed by the spectral type (Tables 1 and 2) and one or two blackbody components.[6] Example spectral energy distributions (SEDs) of A-type and solar-type star-disk systems are shown in Figure 1 as flux density (F_λ) versus wavelength (λ), along with photosphere-subtracted excess flux, and best-fit curves. This approach allows consistent comparison of the results from star to star without invoking the complexities of the disk geometry and the grain optical properties.

A NextGen photosphere and one blackbody contribution (one-belt model) can be thought of as a star with a single ring of dust that achieves a single equilibrium temperature based on its distance from the star. Including a second blackbody curve (two-belt model) describes a star with two rings of dust. The one-belt model has three free parameters and two-belt model has five free parameters: the normalization of the stellar photosphere, the normalization of excess flux density(ies) representing the dust component(s), and the dust temperature(s). As in M09, it is important to leave the normalization of the stellar photosphere a free parameter to allow identification of excess emission at the shortest IRS wavelengths.

In M09 we fit the IRS data from several A-type stars (including HD 138965 in Figure 1) with a power law (or a superposition of blackbodies). However, in many cases, the power law required disk optical depth increasing linearly with

[6] A blackbody fit represents an infinitesimal (very narrow) ring of dust. Continuous disk models of r^{-1} surface density (where r is dust radial location) show that a disk of width of a few times its inner radius does not produce a significant difference in the nominal temperature found from a blackbody fit. For example, a belt of silicate grains around a sun-like star with an inner edge at 3 AU has a similar nominal bulk temperature if the disk extends to 4 AU or 10 AU, while the colder dust starts to make a significant difference in the nominal temperature at $\gtrsim$20 AU.

Table 2
A-type Sample: Stellar Properties and Fitting Results

Name	Spectral Type	Age[a] (Myr)	Dist. (pc)	$F_{\nu,24}$[b] (mJy)	$F_{\nu,70}$[b] (mJy)	$F_{24}/F_\star$	$F_{70}/F_\star$	$L_{d,\mathrm{warm}}/L_\star$	$L_{d,\mathrm{cold}}/L_\star$	T_{warm} (K)	T_{cold} (K)	t_{coll} (10^3 yr)	$M_{\mathrm{min,in}}$ (10^{-8} $M_\oplus$)	M_{pl} (10^{-3} $M_\oplus$)
HD 001404	A2V	...	43.3	154.9 ± 0.8	44.5 ± 6.1	1.29	3.6	2.0×10^{-6}	1.2×10^{-5}	190	62	46	18	...
HD 010939	A1V	320	57.0	108.3 ± 0.6	369.4 ± 6.0	1.59	51.9	6.8×10^{-5}	1.9×10^{-5}	182	55	2	907	1572
HD 023267	A0	80	136.4	36.0 ± 0.3	13.9 ± 3.1	3.58	13.4	1.0×10^{-4}	...	181[c]	...	1	2742	1490
HD 023642	A0V	125	110.4	17.8 ± 0.1	30.6 ± 16.6[d]	1.33	...	1.9×10^{-5}	...	102	...	46	4808	130
HD 023763	A1V	125	144.9	17.8 ± 0.1	43.5 ± 27.1[d]	1.10	...	...	1.8×10^{-5}	...	71	123	10268	104
HD 024141	A5m	...	52.2	66.4 ± 0.5	0.6 ± 11.5[d]	1.43	...	1.9×10^{-5}	...	216	...	2	22	...
HD 024817	A2Vn	400	75.4	45.2 ± 0.3	1.6 ± 12.3[d]	1.59	...	3.4×10^{-5}	...	276	...	1	68	309
HD 028355	A7V	625	49.2	138.3 ± 0.8	182.7 ± 6.5	1.34	16.6	1.6×10^{-5}	1.2×10^{-5}	128	60	10	91	58
HD 030422	A3IV	10	57.5	44.9 ± 0.3	65.6 ± 2.1	1.41	19.6	2.2×10^{-5}	1.6×10^{-5}	173	49	5	143	3
HD 032977	A5V	850	53.2	95.9 ± 0.6	0.6 ± 12.3[d]	1.47	...	2.0×10^{-5}	...	187	...	3	40	116
HD 037286	A2III-IV	...	56.6	65.5 ± 0.4	0.5 ± 10.3[d]	2.32	...	5.2×10^{-5}	...	187	...	2	506	...
HD 038056	A0V	250	132.5	36.4 ± 0.3	48.0 ± 3.4	2.26	28.5	4.5×10^{-5}	4.2×10^{-5}	248	78	1	331	618
HD 038206	A0V	9	69.2	114.7 ± 0.6	370.3 ± 8.1	3.95	118.7	1.7×10^{-4}	1.1×10^{-4}	238	62	0.4	1448	326
HD 070313	A3V	300	51.4	80.8 ± 0.5	209.2 ± 6.2	1.70	42.4	5.2×10^{-5}	2.3×10^{-5}	189	57	2	234	464
HD 071722	A0V	100	71.1	56.6 ± 0.3	136.1 ± 9.5	2.16	50.2	7.9×10^{-5}	3.1×10^{-5}	216	68	1	1001	878
HD 074873	A1V	100	61.1	65.9 ± 0.4	25.4 ± 8.6[d]	1.73	...	3.0×10^{-5}	...	190	...	4	334	89
HD 079108	A0V	320	115.2	45.9 ± 0.3	82.9 ± 3.4	2.05	35.7	4.7×10^{-5}	4.2×10^{-5}	263	70	1	274	824
HD 080950[e]	A0V	80	80.8	116.9 ± 0.6	57.1 ± 2.5	4.09	19.6	6.3×10^{-5}	...	273, 132	...	1	312	351
HD 087696	A7V	900	27.9	213.4 ± 1.0	37.5 ± 5.7	1.29	2.2	1.2×10^{-5}	...	182[c]	...	5	17	32
HD 092536	B8V	50	147.1	47.0 ± 0.3	1.0 ± 19.2[d]	3.09	...	1.1×10^{-4}	...	251	...	1	5800	2983
HD 093738	B9.5V	50	143.9	24.8 ± 0.2	0.3 ± 6.8[d]	1.47	...	2.9×10^{-5}	...	265	...	2	272	71
HD 098673	A7Vn	1000	78.2	42.8 ± 0.3	34.7 ± 5.9	1.73	13.6	1.2×10^{-5}	3.0×10^{-5}	203	60	3	11	34
HD 110411	A0V	10	36.9	147.0 ± 0.7	240.0 ± 5.0	1.68	26.3	4.0×10^{-5}	1.7×10^{-5}	237	74	2	353	21
HD 115892	A2V	350	18.0	698.2 ± 2.7	96.7 ± 4.5	1.20	1.6	7.9×10^{-6}	...	191[c]	...	11	71	22
HD 125283	A2Vn	100	68.5	46.6 ± 0.3	0.5 ± 10.3[d]	1.34	...	1.5×10^{-5}	...	194	...	6	128	23
HD 126135	B8V	15	155.5	23.1 ± 0.2	1.6 ± 3.8[d]	2.71	...	7.5×10^{-5}	...	209	...	3	7937	468
HD 128207	B8V	15	128.5	31.6 ± 0.2	5.8 ± 4.0[d]	1.21	...	9.6×10^{-6}	...	193	...	25	1394	8
HD 132238	B8V	15	191.9	31.8 ± 0.3	3.9 ± 4.3[d]	2.40	...	7.0×10^{-5}	...	240	...	2	4253	354
HD 135379	A3V	600	29.6	341.9 ± 1.5	60.4 ± 87.8[d]	1.73	...	2.8×10^{-5}	...	172	...	4	182	287
HD 135454	B9V	15	137.2	18.2 ± 0.1	0.2 ± 3.4[d]	1.44	...	3.4×10^{-5}	...	324	...	1	229	31
HD 136246	A1V	15	143.5	15.5 ± 0.2	35.7 ± 4.3	1.35	29.8	3.8×10^{-5}	1.2×10^{-5}	215	53	2	257	19
HD 136482[e]	B8/B9V	15	124.5	42.7 ± 0.3	24.0 ± 3.5	3.53	19.3	4.4×10^{-5}	...	281, 112	...	2	870	86
HD 137015	A2V	15	146.6	15.6 ± 0.1	0.2 ± 6.5[d]	1.26	...	1.4×10^{-5}	...	224	...	4	63	2
HD 138923	B8V	15	112.5	59.1 ± 0.4	16.4 ± 6.0[d]	3.46	...	1.5×10^{-4}	...	286	...	0.5	4668	1444
HD 138965	A1V	100	77.3	80.7 ± 0.4	559.4 ± 8.5	3.86	255.8	3.6×10^{-4}	7.9×10^{-5}	172	56	0.4	5929	14129
HD 141378	A5IV	150	49.2	78.3 ± 0.5	225.2 ± 8.9	1.49	41.3	5.4×10^{-5}	1.3×10^{-5}	190	59	1	106	154
HD 142139	A3V	700	66.0	60.8 ± 0.4	43.8 ± 23.6[d]	1.61	...	2.4×10^{-5}	...	177	...	4	141	245
HD 145964	B9V	5	105.8	20.6 ± 0.2	9.1 ± 3.5[d]	1.14	...	8.2×10^{-6}	...	98	...	163	6507	2
HD 153053	A5IV-V	800	50.7	78.8 ± 0.5	156.9 ± 11.5	1.25	23.8	3.7×10^{-5}	5.4×10^{-6}	242	62	1	27	302
HD 159170	A5V	800	48.4	85.9 ± 0.6	34.6 ± 18.7[d]	1.53	...	2.4×10^{-5}	...	209	...	2	32	148
HD 159492	A5IV-V	170	42.2	196.8 ± 1.0	177.6 ± 7.3	2.41	21.1	1.3×10^{-5}	5.1×10^{-5}	162	48	7	48	12
HD 182919	A0V	100	66.9	61.8 ± 0.4	10.8 ± 11.6[d]	1.74	...	3.3×10^{-5}	...	206	...	3	506	162
HD 183324	A0V	10	59.0	51.3 ± 0.4	21.0 ± 3.3	1.21	4.7	9.1×10^{-6}	...	126[c]	...	50	1019	2
HD 191174	A2II-III	...	78.5	38.3 ± 0.3	29.0 ± 6.5	1.92	14.0	1.7×10^{-5}	5.3×10^{-5}	279	63	2	21	...
HD 192425	A2V	120	47.1	131.2 ± 0.8	157.8 ± 7.4	1.74	19.9	2.2×10^{-5}	2.8×10^{-5}	203	57	3	155	54
HD 196544	A2V	...	54.3	75.3 ± 0.5	73.3 ± 6.7	1.63	15.3	1.8×10^{-5}	2.2×10^{-5}	199	70	4	138	...
HD 215766	B9V	100	79.7	63.3 ± 0.4	42.8 ± 7.4	1.97	12.8	1.7×10^{-5}	3.7×10^{-5}	213	77	8	620	82
HD 220825	A0p...	150	49.7	110.6 ± 0.6	30.4 ± 19.2[d]	1.67	...	2.9×10^{-5}	...	204	...	4	467	192
HD 223352	A0V	100	44.0	159.8 ± 0.9	55.5 ± 6.6	1.61	5.4	2.8×10^{-6}	2.5×10^{-5}	195	63	43	55	1
HD 225200	A0V	90	129.0	34.9 ± 0.3	97.0 ± 2.2	1.69	46.9	5.6×10^{-5}	2.9×10^{-5}	243	57	1	451	359

Notes.
[a] Age estimates as in Rieke et al. (2005).
[b] Measured MIPS photometry, not color corrected.
[c] IRS+MIPS 70 μm excess well fit by a single component.
[d] Upper limit.
[e] System with two warm components; the warmest component is used to estimate M_{Pl}.

radius (or faster), which is difficult to understand theoretically. Here, after closer examination of the SEDs (e.g., Figure 1), we chose, instead, the simpler two-belt fits as the default model in all cases.[7] This interpretation is consistent with the steepness of the previously inferred power laws and accounts for the

[7] There are five exceptions, as described in Section 4.2.

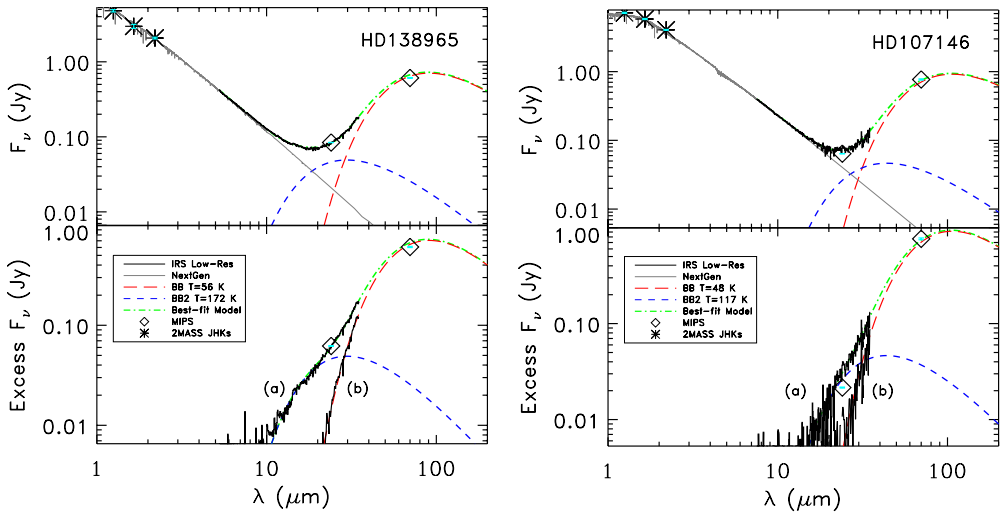

Figure 1. Top: SEDs of two debris systems: A1V HD 138965 (left) and G2V HD 107146 (right). Both are examples of two-belt fits. IRS spectra are shown in solid black and overlaid in gray are the best-fit NextGen stellar atmosphere models. The best-fit warm and cold blackbodies are plotted in blue and red dashed lines, respectively, while the sum of components in dot-dashed green. 2MASS *JHKs* fluxes (Cutri et al. 2003) are plotted as asterisks, and color-corrected MIPS photometry are shown as black diamonds with cyan error bars. Bottom: (a) photosphere-subtracted and (b) photosphere+warm component-subtracted dust emission fluxes vs. wavelength.

Table 3
Summary of Estimated Dust Properties

Debris Systems		Spectral Types	Age (Myr)	$L_d/L_\star$	$T_{\rm warm}$ (K)	$T_{\rm cold}$ (K)	$t_{\rm coll}$ (10^3 yr)	$M_{\rm min,in}$ (10^{-8} $M_\oplus$)	$M_{\rm pl}$ (10^{-5} $M_\oplus$)
19 Solar	Range:	K0V–F5	40–900	4.2×10^{-5} to 9.0×10^{-3}	99–220	47–68	0.04–3	1–2000	4–22000
	Median:	G0	270	2.2×10^{-4}	177	58	0.3	9	80
50 A-type	Range:	B8–A7	5–1000	7.9×10^{-6} to 2.0×10^{-3}	98–324	48–78	0.5–250	17–29000	1–13000
	Median:	A0	100	7.2×10^{-5}	203	62	8	700	120

70 μm detections of all objects previously identified as power-law sources.

4.2. Fitting Results

Results of our fits are summarized in Tables 1 and 2. Close to half (46%) of our sample (24 A-type + 8 solar-type star-disk systems), which make up 86% of the systems seen also at 70 μm, are best described by the two-belt model, with evidence of radially separated inner and outer belts. Five systems however (HD 23267, HD 80950, HD 87696, HD 115892, and HD 118973) have detected 70 μm excess consistent with a single component. For systems not seen at 70 μm, we find that the fit to the IRS emission is similar in temperature to the two-belt model inner components; there appears to be no bias in resultant inner dust temperatures from the absence of a 70 μm detection (be it from limited sensitivity or from the lack of an outer disk component).

Because our A- and solar-type samples are selected on the basis of excess emission in the MIPS 24 μm band, our study emphasizes warm[8] disks. These span a broad range of characteristic dust temperatures, from 98 to 324 K for the A-type sources with a median of 203 K, and from 99 to 220 K for the solar-type sources with a median of 177 K. Table 3 summarizes the characteristic dust temperatures for both spectral samples. Overall, we find that 90% of the inner components have dust temperatures $\geqslant$150 K. Figure 2 emphasizes the similarity in warm grain temperatures for the majority of systems; both A-type and solar-type stars have a median warm disk component close to 190 K.

The outer/cold components of the 24 A-type and 8 solar-type multiple-belt systems have median temperatures of 62 and 58 K, respectively, typical of grains in a Kuiper-like belt.[9] Since emission longward of 70 μm is unknown, we lack specifics on the full radial extent of the outer components; however, the inner edge temperatures of the outer/cold components are strongly constrained by our model fitting.

5. INTERPRETATION AND DISCUSSION

The distribution of dust temperatures for the majority of the warm excesses observed is quite narrow for both A-type and solar-type stars, and more remarkably the median temperatures for the two types are very similar (Figure 2). If dust-producing planetesimal belts were present at similar orbital radii across our B8-K0 stellar sample, the factor of 100 range in stellar luminosities would be expected to produce a factor of three variation in inner belt temperatures. Instead, our SED fitting results show that dust production is favored at the same characteristic temperature across the full range of spectral types. In the discussion below, we implicitly assume that grains producing the warm excess are confined to a narrow range of radii,

[8] We define "warm" as dust of temperature $\gtrsim$100 K.

[9] The exceptions are two multiple-belt A-type systems, HD 080950 and HD 136482, which have two warm components. HD 80950 was observed to be an apparent binary separated by 1.″6 in Moerchen et al. (2010); whether the excess emission is solely attributable to the main star's debris disk is not yet clear.

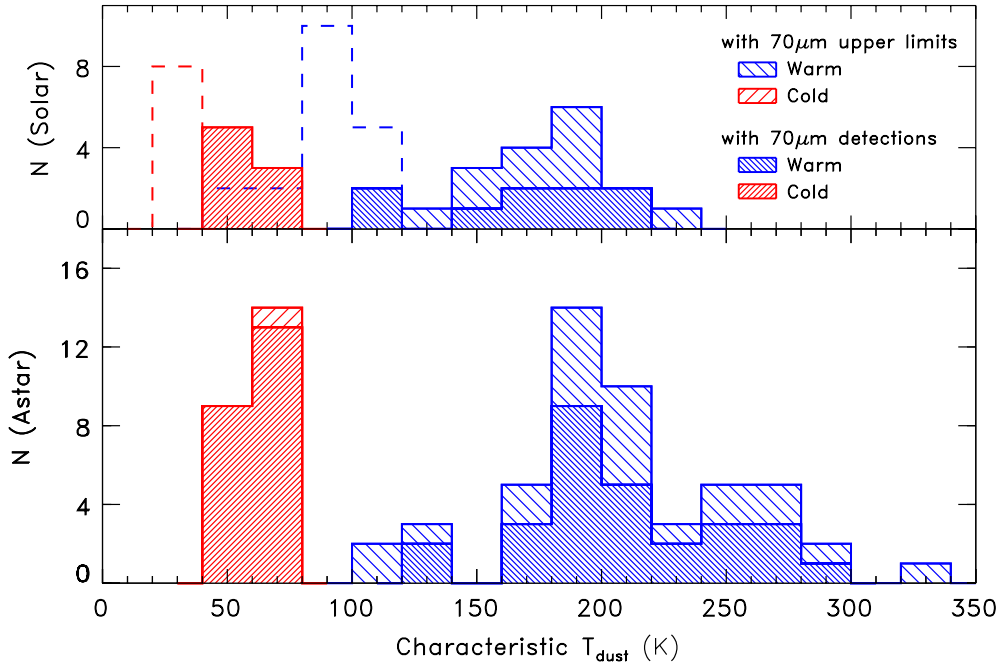

Figure 2. Number counts vs. dust characteristic temperature for the 19 solar-type sources (top) and 50 A-type sources (bottom) in bins of 20 K. Blue and red represent warm- and cold-component counts. Blue and red dashed lines are the expected temperatures if the dust around the solar-type stars were blackbody grains at the median A-sample radial position (∼12 AU). The distribution of warm dust temperatures shows no bias toward systems without 70 μm detections. The high-temperature belts (250–324 K) in the A-star sample may result from the high luminosity of A stars, plus the processing or migration of grains following from evaporation of planetesimals.

consistent with the excellent fit shown in Figure 1. A more complete treatment perhaps leading to more complex radial distributions is deferred to a subsequent paper, as is inclusion of realistic grain size distributions.

Two possible planetesimal populations might explain the favored inner belt temperature of 190 K. The first is that present-day sublimation of icy planetesimals is taking place at around 150 K, and that superheating of the small grains produces the observed characteristic temperature (Campins et al. 1983; Mukai 1996), as Jura (2004) invoked to predict the presence of 25 μm excesses around giant stars, and analogous to cometary disruption and outgassing in our own solar system. A second possibility is that a belt of parent bodies, analogous to the main asteroid belt in our solar system (150–250 K; Low et al. 1984; Kelsall et al. 1998), formed at the observed temperature horizon in the vicinity of the snow line ($T \sim 170$ K; Hayashi 1981; Sasselov & Lecar 2000), and presently produces dust via collisional grinding. In both cases, the uniform grain temperature from star to star results from temperature-dependent processes. We now expand on these two ideas.

In estimating the reservoir of material necessary to produce the warm SEDs, we consider a steady stream of planetesimals. Then, the total minimum mass in cometary or asteroidal material required to maintain the excess during the lifetime (age) of a system is simply $M_{\rm pl} = M_{\rm min,in}$ (age$/t_{\rm coll}$), where $M_{\rm min,in}$ is the minimum dust mass inferred for the inner/warm component today, $M_{\rm pl}$ is mass in planetesimals, and $t_{\rm coll}$ is the grain destruction timescale. The values for $M_{\rm min,in}$ and $t_{\rm coll}$ in Tables 1 and 2 are estimated as in M09 (assuming blackbody grains as small as possible without being blown out from the system, with radial location inferred from the observed dust temperatures, in a ring of uniform density and 10% fractional width, and appropriate stellar properties). We find all systems to be collisionally dominated (e.g., $t_{\rm coll} < t_{\rm Poynting-Robertson}$) with grain lifetimes much shorter than the ages of the stars in our sample. Grain lifetimes range from 40 to ∼2600 yr (median of ∼320 yr) for the solar-type sample and ∼500 to $\sim 2.5 \times 10^5$ yr (median of ∼8000 yr) for debris around the A-type stars. Thus, the minimum dust masses over the ages of the stars (assuming a constant level of excess) are found to be between $\sim 10^{-5}$ and 0.2 $M_\oplus$ (Table 3), with medians of 0.0008 and 0.0012 $M_\oplus$ for debris systems around the solar- and A-type stars, respectively. For solar abundances, if all the heavy elements (Si, Mg, Fe, Al, etc.) are bound in common silicates or oxides, the total mass (including water ice) is ∼2.5 times the mass in the minerals alone. Thus, based on the median values, a minimum mass of ∼0.002 and 0.003 $M_\oplus$ of optimally placed icy planetesimals would suffice to produce the observed dust.

The warm debris may originate from icy planetesimals in roughly circularized orbits (e.g., Jupiter-family comets—JFCs) just exterior to the snow line, analogous to the family of dormant comets in the asteroid belt, or main-belt comets, that appear to have formed locally, remaining in roughly circular orbits, and that may be collisionally activated (Hsieh & Jewitt 2006). Furthermore, according to Cohen & Coker (2000), geochemical and spectroscopic evidence for hydrated minerals on main-belt asteroids is best explained if those asteroids were once bathed in liquid water. To first order, a roughly circularized population of short-period icy planetesimals will produce a small range of dust temperatures because the perturbations caused by multiple close encounters with Jupiter will lead to a gradual increase in eccentricity (Vakhidov 2001; Novaković et al. 2010) until the orbit dips within the snow line, when heating and evaporation will release the observed grains and rapidly destroy the objects. Via dynamical modeling, Nesvorný et al. (2010) argue that asteroidal dust contributes <10% of the zodiacal dust, and that spontaneous disruptions of JFCs, rather than the cometary activity driven by sublimating

volatiles, is the main mechanism liberating particles into the zodiacal cloud today. This is in general agreement with the picture discussed above; a major difference is the higher dust temperatures predicted by Nesvorný et al. (2010). This can be understood because in the lower density environment of the current solar system, Poynting–Robertson drag, rather than collisions followed by expulsion due to radiation pressure, is the main loss mechanism for the grains, which are thus able to drift inward and achieve higher temperatures than is the case in the systems we have studied.

The second possibility to explain the preferred temperature range is that an asteroid belt-like system of parent bodies formed at the observed temperature horizon near the snow line. Kretke & Lin (2007) show that migrating particles in a turbulent protoplanetary disk accumulate near the snow line over a short radial extent and can grow through cohesive collisions. In the presence of an evaporation front, solid particles can grow to almost kilometer sizes within only a few thousand years (Brauer et al. 2008). In this case, the debris dust could be produced by a collisional cascade among bodies left from the original protoplanetary disk. In addition, the jump in surface density of solids just exterior to the snow line makes it the favored location for the formation of gas giants by core accretion (Pollack et al. 1996). If giant planets preferentially form just exterior to the snow line, they may then stir up the remaining reservoir of material just interior. Numerical simulations of terrestrial planet formation support this trend (e.g., Raymond et al. 2005, 2009).

The production of dust and the fraction of stars with debris systems detected at 24 μm (which decays from $\sim$40% at 10 Myr to $<$5% for ages above 1 Gyr (e.g., L. Urban et al. 2011, in preparation; Gáspár et al. 2009; Carpenter et al. 2009)) suggest a reduction with time in the number of planetesimals near the snow line in these systems. This process could take a variety of forms, from dramatic transient episodes like the Late Heavy Bombardment (LHB) through elevated stirring of the planetesimal belts by massive planets, to slow internal erosion of these belts through their internal collisional activity.

In a few well-studied examples (e.g., Fomalhaut (Stapelfeldt et al. 2004), HR 8799 (Su et al. 2009)) as in the solar system, debris rings are shepherded by planets. Fomalhaut and HR 8799 show two belts with exoplanets in between; thus, exoplanets may be responsible for the relative void in dust temperature around 100 K in Figure 2 in some cases.

6. SUMMARY AND CONCLUSIONS

We have analyzed the SEDs of 69 debris disks, previously known to have 24 μm excess, ages up to 1 Gyr, and observed by *Spitzer* IRS and MIPS. These dust distributions have fractional luminosities $\sim 10^{-4}$ to 10^{-5} and are thus considerably more substantial than the dust belts in the solar system. The infrared SED of 32 systems (24 A-type and 8 solar-type) is well fit using two single-temperature blackbody curves which we interpret as two radially distinct dust components. The characteristic dust temperatures ($\sim$190 and $\sim$60 K) for the inner and outer dust components are nearly the same across the full range of spectral types. The common warm dust temperatures in stars of a range of luminosities strongly suggest that the dust is not found at the same radial location around all stars. Instead, we propose that, because the warm belts (91% with $T_{\rm dust} \geqslant 150$ K) have a median temperature slightly warmer than that expected at the snow line, a common grain creation mechanism operates in the inner regions of the star-disk systems—possibly due to sublimation of icy planetesimals crossing the snow line, or from collisional grinding in an asteroid belt-like system at this temperature horizon.

We thank Paul Weissman and Neal Turner (JPL) for their helpful comments and stimulating discussions, and the referee for the careful reading and detailed comments. This work is based on observations made with the *Spitzer Space Telescope*, which is operated by the Jet Propulsion Laboratory, California Institute of Technology, under NASA contract 1407.

REFERENCES

Aumann, H. H., et al. 1984, ApJ, 278, L23
Backman, D. E., Dasgupta, A., & Stencel, R. E. 1995, ApJ, 450, L35
Brauer, F., Henning, T., & Dullemond, C. P. 2008, A&A, 487, L1
Campins, H., Rieke, G. H., & Lebofsky, M. J. 1983, Nature, 301, 405
Carpenter, J. M., et al. 2009, ApJS, 181, 197
Chen, C. H., Sheehan, P., Watson, D. M., Manoj, P., & Najita, J. R. 2009, ApJ, 701, 1367
Cohen, B. A., & Coker, R. F. 2000, Icarus, 145, 369
Cutri, R. M., et al. 2003, 2MASS All Sky Catalog of Point Sources (NASA/IPAC Infrared Science Archive; Pasadena, CA: Caltech), http://irsa.ipac.caltech.edu/applications/Gator/
Fixsen, D. J., & Dwek, E. 2002, ApJ, 578, 1009
Gáspár, A., Rieke, G. H., Su, K. Y. L., Balog, Z., Trilling, D., Muzzerole, J., Apai, D., & Kelly, B. C. 2009, ApJ, 697, 1578
Hayashi, C. 1981, Prog. Theor. Phys. Suppl., 70, 35
Hillenbrand, L. A., et al. 2008, ApJ, 677, 630
Houck, J. R., et al. 2004, ApJS, 154, 18
Hsieh, H. H., & Jewitt, D. 2006, Science, 312, 561
Jura, M. 2004, ApJ, 603, 729
Kalas, P., et al. 2008, Science, 322, 1345
Kelsall, T., et al. 1998, ApJ, 508, 44
Kretke, K. A., & Lin, D. N. C. 2007, ApJ, 664, L55
Low, F. J., et al. 1984, ApJ, 278, L19
Mamajek, E. E., & Hillenbrand, L. A. 2008, ApJ, 687, 1264
Marois, C., Macintosh, B., Barman, T., Zuckerman, B., Song, I., Patience, J., Lafrenière, D., & Doyon, R. 2008, Science, 322, 1348
Moerchen, M. M., Telesco, C. M., & Packham, C. 2010, ApJ, 723, 1418
Morales, F. Y., et al. 2009, ApJ, 699, 1067
Mukai, T. 1996, in ASP Conf. Ser. 104, IAU Colloq. 150: Physics, Chemistry, and Dynamics of Interplanetary Dust, ed. B. A. S. Gustafson & M. S. Hanner (San Francisco, CA: ASP), 453
Nesvorný, D., Jenniskens, P., Levison, H. F., Bottke, W. F., Vokrouhlický, D., & Gounelle, M. 2010, ApJ, 713, 816
Novaković, B., Tsiganis, K., & Knežević, Z. 2010, MNRAS, 402, 1263
Pollack, J. B., Hubickyj, O., Bodenheimer, P., Lissauer, J. J., Podolak, M., & Greenzweig, Y. 1996, Icarus, 124, 62
Raymond, S. N., O'Brien, D. P., Morbidelli, A., & Kaib, N. A. 2009, Icarus, 203, 644
Raymond, S. N., Quinn, T., & Lunine, J. I. 2005, ApJ, 632, 670
Rhee, J. H., Song, I., & Zuckerman, B. 2008, ApJ, 675, 777
Rieke, G. H., et al. 2004, ApJS, 154, 25
Rieke, G. H., et al. 2005, ApJ, 620, 1010
Sasselov, D. D., & Lecar, M. 2000, ApJ, 528, 995
Smith, R., Wyatt, M. C., & Dent, W. R. F. 2008, A&A, 485, 897
Stapelfeldt, K. R., et al. 2004, ApJS, 154, 458
Stern, S. A. 1996, A&A, 310, 999
Su, K. Y. L., et al. 2009, ApJ, 705, 314
Trilling, D. E., et al. 2008, ApJ, 674, 1086
Vakhidov, A. A. 2001, Planet. Space Sci., 49, 793
Werner, M. W., et al. 2004, ApJS, 154, 1